Detailed Structure of Wind and Moisture Fields around the Baiu Frontal Zone over the East China Sea

Shinichiro Maeda[1], Kazuhisa Tsuboki[1], Qoosaku Moteki[2],
Taro Shinoda[1], Haruya Minda[1], and Hiroshi Uyeda[1]
[1]*Hydropheric Atmospheric Research Center, Nagoya University, Nagoya, Japan*
[2]*Institute of Observational Research for Global Change, JAMSTEC, Yokosuka, Japan*

Abstract

An aircraft observation was conducted over the East China Sea to reveal detailed distributions of wind and moisture around the Baiu frontal zone. Using a numerical simulation, the structure of the Baiu frontal zone was examined and four airstreams around the zone were identified: northeasterly, west-southwesterly, and southwesterly along the Baiu frontal cloud zone, as well as southwesterly along the oceanic zone. Each airstream had different characteristics of stratification. These differences and the convergence of the airstreams resulted in two different rainfall areas: a weak and wide rainfall area in the northern part of the cloud zone, and an intense and narrow rainfall area in the southern part.

1. Introduction

The Baiu frontal zone is characterized by a large moisture contrast in the meridional direction (Akiyama 1973; Ninomiya 1984). The Baiu frontal cloud zone has a width of 200–500 km. The rainfall distribution associated with the Baiu front varies with time and space. The rainfall distribution along the Baiu front is strongly affected by the structures of the wind field and the moisture distribution. The rainfall systems that reach the Okinawa region develop first in the East China Sea. The detailed structure of the Baiu frontal zone over the sea is not well clarified because of its complicated structure and rapid development over the sea. There have been a few observations to study the detailed wind and moisture distributions over the East China Sea.

Moteki et al. (2004a, b) reported a strong rainband, which they called a water vapor front, to the south of a main precipitation system of the Baiu front over the East China Sea. Three types of synoptic wind and moisture fields (oceanic moist air, continental moist air, and northern cold pool) composed the main Baiu front and the water vapor front. On the other hand, a low-level wind shear line was observed at 200–300 km north of the surface Meiyu/Baiu front (Chen et al. 1998). These results indicate that the wind and moisture fields around the Baiu frontal zone may have diverse distributions.

The purpose of this study is to reveal detailed structures of wind and moisture fields controlling the rainfall distribution around the Baiu frontal zone. We conducted an aircraft observation of the Baiu frontal zone over the East China Sea on 23 June 2005. In order to understand the observed structure, we carried out numerical simulations using a cloud-resolving model.

2. Observations and modeling

2.1 Aircraft observation

On 23 June 2005, we performed an aircraft observation of the Baiu frontal zone over the East China Sea almost along 125.9°E. The flight path is indicated in Fig. 1. The observed variables are temperature (T), dewpoint temperature (Td), pressure (P), and wind (U, V, W) at a height of 500 m. The flight altitude was selected to observe water vapor in the lower atmosphere. Dropsonde soundings were carried out from an altitude of about 12 km. Locations are indicated in Fig. 2a, and time and positions are summarized in Table 1.

2.2 Numerical simulations

To help our understanding of the detailed structure of the Baiu frontal zone, we performed numerical simulations using the Cloud Resolving Storm Simulator (CReSS; Tsuboki and Sakakibara 2002). CReSS is a non-hydrostatic model using bulk cold rain cloud physics. Model domains are shown in Fig. 1, and detailed settings of the simulations are summarized in Table 2. Lateral boundary conditions of the 4-km simulation were obtained from JMA-RSM (Japan Meteorological Agency, Regional Spectral Model) model output.

3. Meridional distribution

While the aircraft flew from north to south, the rain-

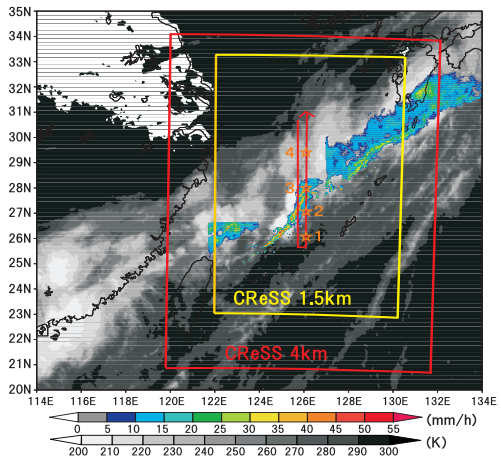

Fig. 1. GOES IR1 (gray shadings) and Japan Meteorological Agency (JMA) radar (color shadings) at 0300UTC on 23 June 2005. The flight path is shown by the red line, with dropsonde positions indicated by the orange stars. The red and yellow rectangles indicate simulation domains with horizontal resolutions of 4 km and 1.5 km, respectively.

Table 1. Observation time and positions.

Name	TIME (UTC)	Latitude, Longitude
500 m Flight	3:03–4:17	30.8N–25.5N, 125.9E
Dropsonde 1	4:38	25.93N, 125.85E
Dropsonde 2	5:02	27.03N, 125.83E
Dropsonde 3	5:26	27.97N, 125.82E
Dropsonde 4	5:47	29.47N, 125.93E

Corresponding author: Shinichiro Maeda, Hydropheric Atmospheric Research Center, Nagoya University, Furo-cho, Chikusa-ku, Nagoya 464-8601, Japan. E-mail: maeda-shin-3.8z@m9.dion.ne.jp.

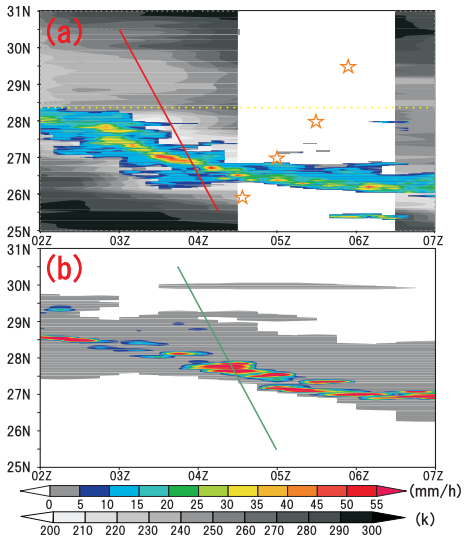

Fig. 2. (a) Time-latitude cross-section of rainfall intensity and cloud zone at 125.9°E. The color scale shows observed rainfall intensity obtained from the JMA radar. The gray scale shows Tbb of GOES IR1. The red line indicates the flight path, and the orange stars show dropsonde positions. (b) Time-latitude cross-section of rainfall intensity obtained from the CReSS 1.5-km simulation at 125.5°E; the slight shift in longitude is explained in Section 4.1. The green line (virtual flight path) corresponds to the flight path (the red line) in (a).

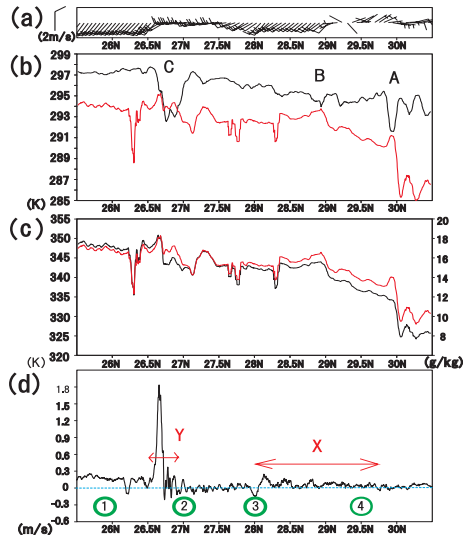

Fig. 3. Meridional profiles at an altitude of 500 m along 125.9 °E of (a) wind, (b) temperature (black curve) and dewpoint temperature (red curve), and (c) equivalent potential temperature (black curve) and mixing ratio of water vapor (red curve), (d) vertical wind velocity. In (b), dewpoint temperature is higher than temperature at C, owing to the ventilation effect. In (d), the green circles with numbers show the positions of dropsondes.

Table 2. Detailed configurations of CReSS 4 km and CReSS 1.5 km simulations.

Grid scale (km)	Grid points	Initial data	Initial time
4.0×4.0×0.50	293×360×36	JMA-RSM	18UTC22
1.5×1.5×0.32	420×600×36	4-km run	21UTC22

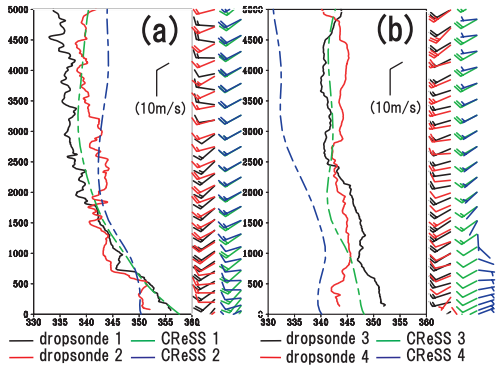

Fig. 4. Equivalent potential temperature (curves) and horizontal wind profiles (arrows) of 4 dropsondes. (a) Dropsondes 1 (black) and 2 (red). Green and blue (dashed lines/arrows) show the simulation results that correspond to dropsondes 1 and 2, respectively. (b) Dropsondes 3 (black) and 4 (red). Green and blue (dashed lines/arrows) show the simulation results that correspond to dropsondes 3 and 4, respectively.

fall system in the Baiu frontal zone was changing drastically. We, therefore, took into account the temporal variation in the precipitation area. Figure 2a shows the cloud and rainfall areas in the time-space domain. The red line and stars indicate the 500-m flight path and dropsonde positions, respectively. There was no radar echo north of 28.3N which is the limit of the radar range. GOES IR1 is shown a half-hour delayed because it took about an hour for the satellite to cover the whole range. GOES had no data from 0500 to 0700 UTC. The heavy rainfall moved about 1 degree to the south during the aircraft observation. Figure 2b shows the simulation result, which is discussed in detail below.

Figure 3 shows the results of the flight at an altitude of 500 m. There were two major wind shear lines at 29.3 °N between northeasterly and southwesterly and at 26.7 °N between westerly and southwesterly (Fig. 3a). There were three saturated points in Fig. 3b: A (29.9°N), B (28.9 °N), and C (26.8°N). Large gradients of equivalent potential temperature (θ_e) and water vapor mixing ratio (qv) were present near A (29.9°N; Fig. 3c). There were two major ascending areas (Fig. 3d): The area X (28–29.8°N) was weak and wide, while the area Y (26.2–26.8°N) was strong and narrow.

The surface Baiu front was located at 28°N on the JMA weather chart. The ascending area X in Fig. 3d corresponded to the cloud zone around 28.5–30°N in Fig. 2a, where weak rainfall was observed. The ascending area Y in Fig. 3d corresponded to the heavy rainfall area shown in Fig. 2a, which was about 300 km south of the intense moisture gradient.

Dropsonde sounding results are shown in Fig. 4. Figure 4a shows the θ_e profiles of Dropsondes 1 and 2, located to the south and north of the heavy rainfall area (Fig. 2a), respectively. Dropsonde 1 had a larger θ_e than Dropsonde 2 below 500 m, although the difference between them was small at 500 m. The convective instability was more intense to the south of the heavy rainfall area than to the north. The values of CAPE observed by Dropsondes 1 and 2 were about 1800 and 800 J kg^{-1}, respectively.

Figure 4b shows the θ_e profiles of Dropsondes 3 and 4. There was no precipitation at the location of Dropsonde 3. The rainfall or cloud area around Dropsonde 4 was not observed due to the lack of radar and satellite data. Dropsonde 3, with almost the same profile as that of Dropsonde 2, showed weak convective instability. Dropsonde 4 displayed a convective neutral profile except for the lower-level cold and dry inflow from the east below 1 km. The values of CAPE observed by Dropsondes 3 and 4 were about 800 and 0 J kg^{-1}, respectively.

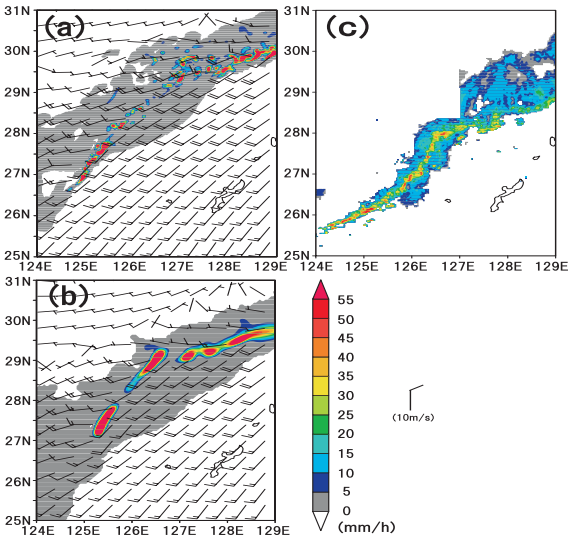

Fig. 5. Rainfall intensity obtained from the 1.5-km simulation at 7 hrs from the initial time (a) and 4-km simulations at 10 hrs (b), and rainfall intensity from the JMA raingauge-calibrated radar observation at 0400 UTC (c). Arrows show wind at a height of 500m.

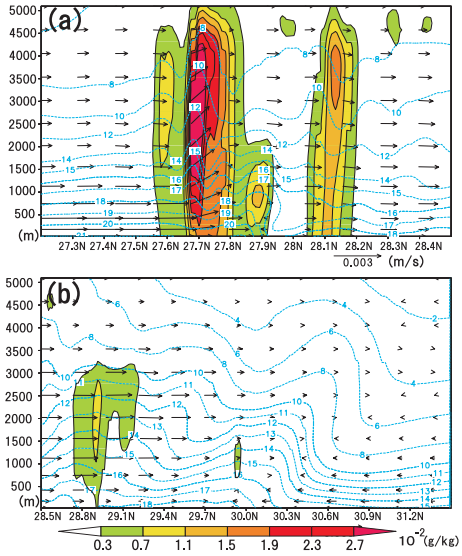

Fig. 7. Vertical cross-sections along the green line in Fig. 2b. (a) Southern rainfall area (Y). (b) Northern rainfall area (X). Color shadings indicate mixing ratio of hydrometeors. Dashed contours are the mixing ratio of water vapor. Vectors indicate v and w components of the velocity.

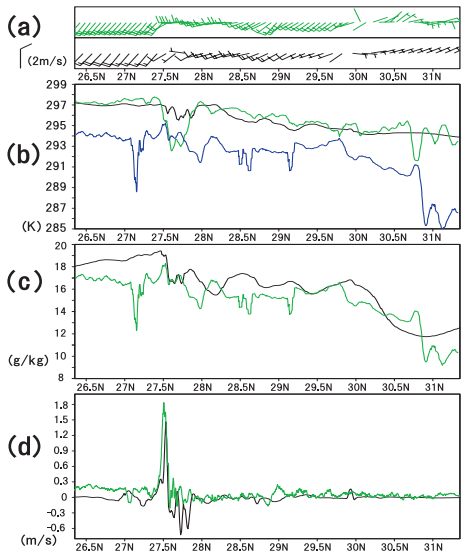

Fig. 6. Meridional profiles at 500 m obtained from the aircraft observation and the 1.5-km CReSS simulation. Green and blue colors show the observations, and black shows the 1.5-km simulation result. (a) Wind, (b) temperature and dewpoint temperature (observation), (c) equivalent potential temperature, and (d) vertical wind velocity. Observational profiles were displaced 0.8 degrees to the north to compare with the simulation result.

4. Simulation results

4.1 Verification by observations

We verify the simulation results using the radar echo in detailed analysis. Figure 5 shows the rainfall intensity obtained from simulations and the JMA radar observations. The distributions of simulated rainfall are similar to those of the radar echo in shape, while the location of the rainband is slightly to the north of the observed one. This difference is also seen in Fig. 2, while Figs. 2a and 2b show a similar transition pattern of the heavy rainfall area. Although the locations of the heavy rainfall in the simulations are slightly different from those observed, the essential features of the Baiu frontal zone are successfully simulated. Considering the difference, we set the virtual flight time in the simulation for 0345–0500UTC and the virtual location at 125.5°E (shown by the green line in Fig. 2b). Figure 6 compares the profiles of the CReSS 1.5-km results with those of the observed results along the red and green lines in Figs. 2a and 2b, respectively. Although the location of the ascending area Y was not exactly simulated, the profile was similar enough for comparison with that from the observation. In order to compare the distribution of typical ascending areas and wind shears clearly, observed profiles were displaced 0.8° to the north. The simulation results had the similar characteristics as those of the observed results: two ascending areas and a strong moisture gradient. Furthermore, we will examine the similarity of vertical profiles (Figs. 4a and 4b). Figure 4a shows quite similar profiles between observations and simulations. Although the simulated θ_e profiles in Fig. 4b are 3–4K lower than that of observations, their profile patterns especially in the lower levels are almost the same. Thus, the CReSS results simulated the observed Baiu frontal zone well, not only in terms of the horizontal distribution but also of the vertical and temporal variation.

4.2 Vertical structures

Figure 7 shows the vertical cross-sections along the virtual flight path (the green line in Fig. 2b). In the area Y (Fig. 7a), the heavy and narrow rainfall areas are simulated. The atmosphere to the south of the heavy rainfall area is much moister than that to the north below 1.5 km. The same feature was found in the θ_e profile of Dropsondes 1 and 2. In the area X (Fig. 7b), the shallow convective rainfall area is simulated. It shows a strong horizontal qv contrast and wind shear around 30 °N, corresponding to the Baiu front shown in the weather chart. Cold and dry air is present to the north of 30°N. The air to the south of the cloud area slowly ascends over the northern air mass. This structure corresponds to the θ_e and the wind features shown in the lower level of the profile, observed by Dropsonde 4 (Fig. 4b).

4.3 Large-scale wind field

Finally, we examined the environmental wind field to understand the structure of the observed wind and moisture fields. We made a back-trajectory analysis (Golding 1984) using the outputs of the 4-km simulation (Fig. 8). The back-trajectories started at 0300UTC from an altitude of 500 m. The results revealed significant structures of wind fields around the Baiu frontal zone. We found four major airstreams in the lower level: the northeasterly (NE-ly), the west-southwesterly (WSW-ly), and two southwesterlies (SW-ly 1, SW-ly 2). NE-ly and SW-ly 2 come from the edge of northern and southern high pressure, respectively. WSW-ly and SW-ly 1 merged around 26N, 122E where a meso-scale cloud cluster is found in Fig.1. The convergence/confluence area between SW-ly 1 and SW-ly 2 corresponds to the southern heavy rainfall area (Y), while the convergence/confluence area between NE-ly and WSW-ly corresponds to the northern ascending area (X).

5. Discussion

The Baiu frontal zone in the present study had four major airstreams. The properties of these airstreams were observed by the dropsondes (Fig. 4). The NE-ly was cold and dry in the lower level, as shown by Dropsonde 4. The WSW-ly and the SW-ly 1 were characterized by comparatively moist and weak convective instability, as shown in the profiles of Dropsondes 3 and 2, respectively. The SW-ly 2 was very moist below 500 m, and had intense convective instability, as shown by Dropsonde 1.

In the ascending area X, weak convective rainfall occurred due to the weak convective instability of the WSW-ly, which ascended over the NE-ly. In the ascending area Y, intense convective rainfall occurred owing to the intense convective instability of the SW-ly 2, which ascended over the SW-ly 1, and to the ample moisture supply from the south in the lower level.

6. Summary and conclusions

An aircraft observation was performed on 23 June 2005 to study detailed structures of wind and moisture fields in the Baiu frontal zone. Based on the flight data at the altitude of 500 m, we found two areas of ascending and wind shears. They correspond to two rainfall areas: One was a weak rainfall area, which corresponded to a large moisture gradient; the other area, located 400 km south of the weak rainfall area, had a weak moisture contrast and heavy rainfall. Using dropsonde soundings, vertical profiles on the north and south sides of each rainfall area were successfully observed. Each side of the rainfall area had different properties of wind and moisture.

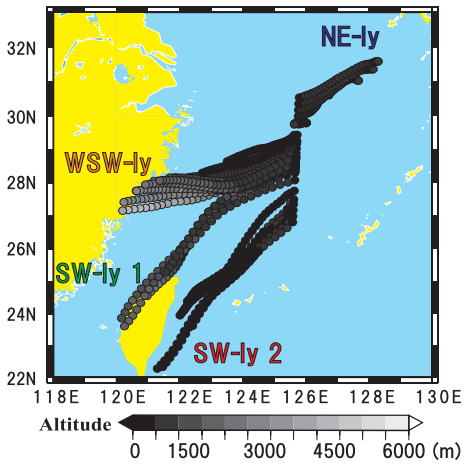

Fig. 8. Back-trajectories traced from 126°E and 500 m. Gray scale of tracer particles shows the altitude of each air mass.

In order to understand the observations, we performed numerical simulations using CReSS. The wind field structure around the Baiu frontal zone was revealed from vertical sections and back-trajectory analysis. There were four airstreams: the northeasterly (NE-ly), the west-southwesterly (WSW-ly), the southwesterly 1 (SW-ly 1), and the southwesterly 2 (SW-ly 2). The WSW-ly ascended weakly over the NE-ly, which was observed as the ascending area X. The SW-ly 1 and the SW-ly 2 strongly converged and the SW-ly 2 ascended over the SW-ly 1, which formed the ascending area Y.

Dropsonde profiles showed the properties of these airstreams. The NE-ly was cold and dry. The WSW-ly and the SW-ly 1 were characterized by comparatively moist and weakly convective instability. The SW-ly 2 was characterized by very moist and strong convective instability. These characteristics resulted in two different types of precipitation. Northern weak rainfall was formed by the weak convective instability of the weakly ascending WSW-ly. Southern heavy rainfall was due to the intense convective instability and ample moisture supply from the SW-ly 2.

Acknowledgments

The authors would like to thank all the participants in the aircraft observation. Data sets for radar, sonde (Taipei, Ishigaki Island, and Kagoshima), and GOES IR1 were provided by the Japan Meteorological Agency, University of Wyoming, and Kochi University, respectively. The authors extend their thanks to Prof. D.-I. Lee, Pukyong National University, for providing sounding data. This study was supported by a Grant-in-Aid for Scientific Research by the Ministry of Education, Culture, Sports, Science, and Technology of Japan.

References

Akiyama, T., 1973: The large-scale aspects of the characteristic features of the Baiu front. *Pap. Meteor. Geophy.*, **24**, 157–188.

Chen, S.-J., Y.-H. Kuo, W. Wang, Y. Tao, and B. Cui, 1998: A modeling case study of heavy rainstorms along the Mei-Yu front. *Mon. Wea. Rev.*, **126**, 2330–2351.

Golding, B., 1984: A study of the structure of mid-latitude depressions in a numerical model using trajectory techniques. I: Development of ideal baroclinic waves in dry and moist atmospheres. *Quart. J. Roy. Meteor. Soc.*, **11**, 847–879.

Moteki, Q., H. Uyeda, T. Maesaka, T. Shinoda, M. Yoshizaki, and T. Kato, 2004a: Structure and development of two merged rainbands observed over the East China Sea during X-BAIU-99 Part I: Meso-β-scale structure and development process. *J. Meteor. Soc. Japan*, **82**, 19–44.

Moteki, Q., H. Uyeda, T. Maesaka, T. Shinoda, M. Yoshizaki, and T. Kato, 2004b: Structure and development of two merged rainbands observed over the East China Sea during X-BAIU-99 Part II: Meso-α-scale structure and building-up process of convergence in the Baiu frontal region. *J. Meteor. Soc. Japan*, **82**, 45–65.

Ninomiya, K., 1984: Characteristics of Baiu front as a predominant subtropical front in the summer northern hemisphere. *J. Meteor. Soc. Japan*, **62**, 880–894.

Tsuboki, K., and A. Sakakibara, 2002: *Large-scale parallel computing of Cloud Resolving Storm Simulator*. H. P. Zima, et al., Eds., High Performance Computing, Springer, 243–259.

Manuscript received 9 September 2008, accepted 29 November 2008
SOLA: http://www.jstage.jst.go.jp/browse/sola/